Thermoelectric Power Factor of Low Dimensional Silicon Nanowires

Neophytos Neophytou and Hans Kosina

Institute for Microelectronics, TU Wien, Gußhausstraße 27-29/E360, A-1040 Wien, Austria
e-mail: {neophytou|kosina}@iue.tuwien.ac.at

Abstract. We analyze the thermoelectric power factor in ultra-narrow low-dimensional silicon nanowires (NWs) by employing atomistic considerations for the electronic structures and linearized Boltzmann transport theory. We consider different transport orientations and both n-type and p-type NWs. We show that the NW properties are highly anisotropic, especially for p-type, and as the diameter is reduced from D=12nm (bulk-like) down to D=3nm (1D-like), changes appear in the dispersions of the NWs, that can affect the power factor (σS^2). We show that the conductivity has a stronger influence on the power factor compared to the Seebeck coefficient under geometrical changes. In the case of p-type NWs, bandstructure changes through confinement can improve the carrier velocities and result in power factor improvements.

Keywords: thermoelectrics, Si nanowires, atomistic, Boltzmann
PACS: 84.60.Rb, 72.15.Jf, 73.63.Nm

INTRODUCTION

Low dimensional silicon channels, such as nanowires (NWs) and 2D ultra-thin-body (UTB) layers, have attracted significant attention as efficient thermoelectric materials since the work of Hicks and Dresselhaus [1], who pointed out that low dimensionality can be beneficial to the Seebeck coefficient. Recently, Boukai *et* al. [2], and Hochbaum *et* al. [3] showed that it is indeed possible to achieve ZT~0.5 at room temperature in Si NWs of diameters less than 50nm (compared to bulk Si ZT_{bulk}~0.01). This, however, was mostly a result of significant reduction in the lattice part of the thermal conductivity, k_l. In nanostructures and low-dimensional materials, narrow features sizes not only reduce phonon transport, but they also reduce the electronic conductivity (σ). On the other hand, high power factor is still important in achieving high thermoelectric performance. Proper optimization of the power factor is therefore essential, and for this, proper theoretical tools are needed to provide design guidance.

In this work, we calculate the thermoelectric power factor of scaled silicon NWs using the $sp^3d^5s^*$-spin-orbit-coupled (SO) atomistic tight-binding (TB) model and Boltzmann transport. We examine cylindrical n-type and p-type NWs of diameters from D=3nm (ultra-scaled) to D=12nm (electrically approaching bulk), in [100], [110] and [111] transport orientations. We show that especially for p-type NWs, the power factor is strongly anisotropic. As the diameter is reduced, changes in the dispersions of the NWs influence the electronic properties significantly. This can provide optimization strategies for high efficient thermoelectric NW devices.

APPROACH

The $sp^3d^5s^*$-SO TB model [4] accurately captures the electronic structures and inherently includes the effects of quantum confinement. It represents a compromise between computationally expensive fully *ab-initio* methods, and numerically inexpensive but less accurate effective mass models. Our calculations can include up to 5500 atoms, a challenging, but achievable computational task within this model. The electronic structures of the NWs are different in different orientations and therefore the NWs have different electronic properties. The electronic structures are also sensitive to the diameter of the NW, which makes their properties diameter dependent as well.

In some cases, reduction in the diameter can actually improve the performance of the NW. Figure 1a shows the bandstructure carrier velocities of NW categories in which the velocity undergoes an improvement with diameter reduction. These are the p-type [111] and [110] NWs, and the n-type [110] NWs. In the case of the p-type NWs, the carrier velocity can increase as much as ~2X with diameter reduction.

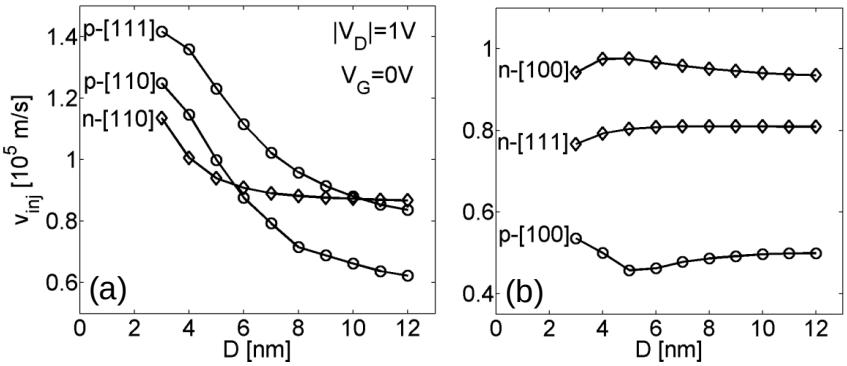

FIGURE 1. The bandstructure velocities of cylindrical NWs as a function of the diameter under non-degenerate, ballistic transport conditions. n- and p-type NWs in [100], [110] and [111] transport orientations are shown. (a) NW categories for which the carrier velocity increases with confinement. (b) NW categories for which the carrier velocity remains rather constant.

On the other hand, for the n-type [100] and [111] NWs, and the p-[100] NWs, the carrier velocities remain constant with diameter. Possibilities for performance optimization are therefore available, both with regards to orientation, as well as diameter. This is particularly important for nanostructures in which narrow feature sizes are favorable in order to reduce the phonon part of the thermal conductivity, k_l.

The electrical conductivity and Seebeck coefficient follow from linearized Boltzmann theory as:

$$\sigma = q_0^{\,2} \int_{E_0}^{\infty} dE \left(-\frac{\partial f_0}{\partial E} \right) \Xi(E), \tag{1}$$

$$S = \frac{q_0 k_B}{\sigma} \int_{E_0}^{\infty} dE \left(-\frac{\partial f_0}{\partial E} \right) \Xi(E) \left(\frac{E - E_F}{k_B T} \right), \tag{2}$$

where the transport distribution function is defined as [5]:

$$\begin{aligned} \Xi(E) &= \sum_{k_x, n} v_n^{\,2}(k_x)\, \tau_n(k_x)\, \delta\left(E - E_n(k_x)\right) \\ &= \sum_{n} v_n^{\,2}(E)\, \tau_n(E)\, g_{1D}^{n}(E). \end{aligned} \tag{3}$$

Here, $v_n(E) = \partial E_n / \hbar \partial k_x$ is the bandstructure velocity, $g_{1D}^{n}(E) = 1/\left(2\pi\hbar v_n(E)\right)$ is the density of states for the 1D subbands (per spin), $\tau_n(k_x)$ is the momentum relaxation time for a state with k_x in subband n, and E_F is the Fermi level. We use Fermi's Golden Rule to extract the transition rate for a carrier in an initial state k_x in subband n to a final state k_x' in subband m. Elastic and inelastic scattering processes are considered. We consider all bulk electron-phonon scattering mechanisms. Although the NW dispersions are all projected onto the 1D k-space from the bulk 3D k-space, we carefully select the final scattering states for each initial state according to the selection in bulk Si processes. As an example, we demonstrate the selection of the final scattering states of a particular state k_x in subband n for the D=3nm [110] n-type and p-type NWs. Their dispersions are shown in Fig. 2a and Fig. 2b respectively. The dispersion of the n-type NW consists of six valleys, originating from the six equivalent energy ellipsoids of Si conduction band. These are projected onto the 1D k-space, and in the [110] orientation, three two-fold degenerate valleys are formed as shown in Fig. 2a. From bulk Si scattering selection "rules" the elastic processes are only intra-valley, whereas inelastic ones are only inter-valley. Since these two-fold degenerate valleys originate from different conduction band ellipsoids, we allow scattering within these valleys as follows: i) For elastic scattering, in a specific valley (either Γ or off-Γ) transitions are allowed only from even to even and odd to odd subband numbers. ii) Inelastic inter-valley scattering transitions are allowed from even to odd and vice versa only within a specific valley (Γ or off-Γ). For inelastic transitions between the different valleys as shown in Fig. 2a, the final state of each scattering event is selected according to whether the process is of *f*- or *g*-type. All six relevant phonon modes in Si are included [6]. Similar procedure is followed for the final state selection in n-type NWs in the other transport orientations. For p-type, the selection rules are simpler. We allow all inter-band and intra-band

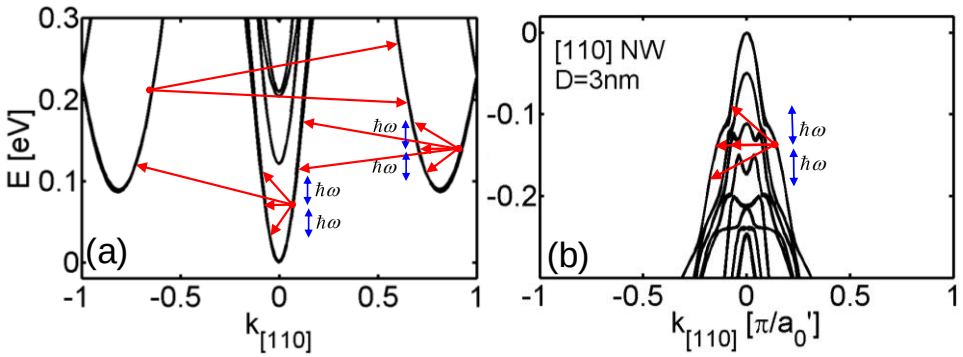

FIGURE 2. The dispersion of the [110] NW of D=3nm. Elastic and inelastic transitions are shown. (a) Conduction band. (b) Valence band.

scattering within all subbands as shown in Fig. 2b. The full description of the procedure is described in [7].

RESULTS AND DISCUSSION

From Eqs. 1 and 2 it can be deduced that the electrical conductivity increases exponentially as the Fermi level moves closer to the band edges, whereas the Seebeck coefficient decreases linearly, at least for non-degenerate conditions. At a specific carrier concentration, the position of the Fermi level with respect to the band edges (η_F) will be determined by the density of states (DOS) of the NW dispersions. The DOS is determined by the effective mass of the subbands and their degeneracies. The η_F of NWs in the [100], [110], and [111] transport orientations, at carrier concentrations of 10^{18}/cm^3 vs. the NW diameter is shown in Fig. 3a and 3b for n-type and p-type NWs, respectively. At larger diameters, the dispersions approach the bulk electronic structure and bulk DOS, and therefore η_F is the same for NWs is all orientations. As the diameter is reduced, the dispersions are different for each orientation, and η_F changes. For the narrowest D=3nm NWs, in the n-type case the [110] oriented NW has a smaller η_F, whereas for the p-type NWs the [111] and [110] NWs have the smallest η_F. The η_F for NWs with lighter effective masses (and higher carrier velocities), are smaller. This provides higher electrical conductivity, but also lower Seebeck coefficient. Since the electrical conductivity is benefited exponentially from this reduction in η_F whereas the Seebeck coefficient is degraded linearly, the diameter reduction will influence the power factor more through changes in the conductivity than the Seebeck coefficient.

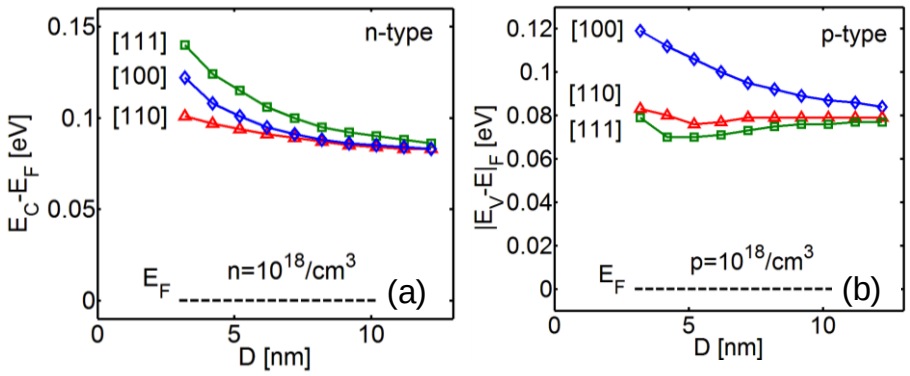

FIGURE 3. The difference of the conduction/valence band minimum/maximum from the Fermi level (η_F)assuming a carrier concentration 10^{18}/cm^3 for NWs in the [100] (diamond-blue), [110] (triangle-red) and [111] (square-green) transport orientations versus the NWs' diameter. (a) n-type NWs. (b) p-type NWs.

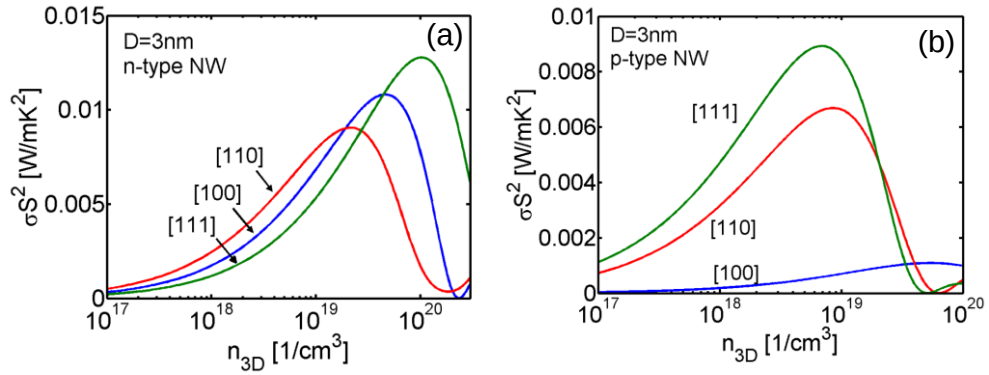

FIGURE 4. The phonon-limited thermoelectric power factor for NWs with D=3nm in [100] (blue), [110] (red) and [111] (green) transport orientations. (a) n-type NWs. (b) p-type NWs

This is indicated in Fig. 4, which shows the power factor versus carrier concentration for the D=3nm NWs in the three orientations examined. Figure 4a shows the power factor for n-type NWs and Fig. 4b for p-type NWs. In the non-degenerate limit, for carrier concentrations below 10^{19}/cm^3, the power factor is larger for the NWs with smaller η_F, (i.e. [110] n-type NW), although at higher concentrations the order can change. N-type NWs do not show large anisotropy, but the p-type NWs are highly anisotropic, with the [111] and [110] NWs having almost an order of magnitude higher performance compared to the [100] NWs. The first two NWs have a much larger conductivity because: i) their carrier velocity is highly advantageous and increases with diameter reduction (Fig. 1a), and ii) at a specific carrier concentration their band edges reside closer to the Fermi level. This is reflected on the higher power factor as well.

CONCLUSIONS

We analyze the thermoelectric power factor in ultra-narrow silicon nanowires (NWs) by employing atomistic considerations for the electronic structures and linearized Boltzmann transport theory. We consider different transport orientations and both n-type and p-type NWs. We show that as the diameter of the NWs is reduced from D=12nm (bulk-like) down to D=3nm (1D-like), the NW carrier velocities, the DOS, and the position of the band edges with respect to the Fermi level change, and influence the power factor. The power factor is highly anisotropic especially for p-type NWs, for which the D=3nm [111] and [110] NWs have ~10X higher performance than the [100] NWs. We also indicate that geometrical changes affect the conductivity more than they affect the Seebeck coefficient and that the conductivity finally determines the power factor. Performance optimization strategies can be identified to improve the design of low-dimensional thermoelectrics.

ACKNOWLEDGMENTS

This work was supported by the Austrian Climate and Energy Fund, contract No. 825467.

REFERENCES

1. L.D. Hicks, and M. S. Dresselhaus, *Phys. Rev. B*, vol. 47, no. 24, p. 16631, 1993.
2. A.I. Boukai, Y. Bunimovich, J. T.-Kheli, J.-K. Yu, W. A. Goddard III, and J. R. Heath, *Nature*, vol. 451, pp. 168-171, 2008.
3. A. I. Hochbaum, R. Chen, R. D. Delgado, W. Liang, E. C. Garnett, M. Najarian, A. Majumdar, and P. Yang, *Nature*, vol. 451, pp. 163-168, 2008.
4. T. B. Boykin, G. Klimeck, and F. Oyafuso, *Phys. Rev. B*, vol. 69, no. 11, pp. 115201-115210, 2004.
5. T. J. Scheidemantel, C. A.-Draxl, T. Thonhauser, J. V. Badding, and J. O. Sofo, *Phys. Rev. B*, vol. 68, p. 125210, 2003.
6. C. Jacoboni and L. Reggiani, *Rev. Mod. Phys.*, vol. 55, 645, 1983.
7. N. Neophytou and H. Kosina, *Phys. Rev. B*, vol. 84, p. 085313, 2011.